SIMULATION OF DIURNAL VARIATION OF SUB-IONOSPHERIC VLF TRANSMITTER SIGNALS USING MACHINE LEARNING APPROACH

K. GIRI[1], S. PAL[2,*], T. K. BISWAS[1], S. K. MIDYA[3]

[1]Department of Computer Science, National Institute of Technical Teachers Training and Research, Block - FC, Sec - III, Saltlake Kolkata-700106, India
E-mail: kinsuk@nitttrkol.ac.in
[2]Department of Physics, Srikrishna College, Nadia, West Bengal, India
E-mail: myselfsujay@gmail.com (*corresponding author)
[3]Department of Atmospheric Sciences, University of Calcutta, Kolkata, India
E-mail: drskm06@yahoo.co.in

Received: *February 8, 2021* (RJP v2.0 r2018a)

Abstract. This paper shows simulation models for diurnal variation of sub-ionospheric Very Low Frequency (VLF) signals using machine learning approach. Recording of VLF transmitter signals using a ground-based radio receiver provides a beautiful and cost-effective way of monitoring lower ionosphere (D/E regions) in the altitude range (60-90 km). VLF signals respond to the ionization variations due to the Sun and other terrestrial or extra-terrestrial sources. Consequently, it has many applications in remote sensing of the lower ionosphere. Therefore, predicting or simulating the diurnal variation of VLF transmitter signals using past data will help to understand the variability of the ionosphere. Here, the VLF signal from the Indian transmitter VTX (18.2 kHz) received at Kolkata is used for the training, validating, and testing purposes in the machine learning models. Two predictive models, multiple linear regression (MLR) and artificial neural network (ANN) have been built and Pearson correlation coefficients outside the training range are obtained as R=0.94 and R=0.93 respectively for the two models. Variation of the VLF transmitter signal is also calculated using the well-known Long Wave Propagation Capability (LWPC) code coupled with the International Reference Ionosphere (IRI-2016) model and the same is compared with the MLR and ANN model predictions. Both the MLR and ANN models are found to be performing better than the LWPC simulation.

Key words: VLF Remote Sensing; Machine Learning; D-region Ionosphere; Sub-ionospheric VLF signals;.

1. INTRODUCTION

Very Low Frequency (VLF) radio signal in the frequency range between 3-30 kHz is one of the important tools to monitor the lower ionosphere continuously. VLF signals which are originated from the lightning discharge or the navigational transmitters around the world can be received by a suitable antenna-receiver system. Due to their low attenuation rate, VLF signals propagate to long distances in the earth-ionosphere waveguide with multiple reflections in the earth's surface and iono-

sphere. Therefore, it preserves the information about the reflecting surfaces. Properties of the lower ionosphere can be studied continuously by recording the VLF signals. VLF signals recorded at any place show variation in different time scales ranging from seconds, hourly, daily, monthly, seasonal, yearly to long-term. Various sources such as lightning, solar x-ray and UV, flares, geomagnetic storms, cosmic rays, and solar cycle are responsible for such variations in VLF signals in different time scales ([1] and references therein). In addition to such sources, some meteorological sources, such as tropical cyclones, stratospheric warming events ([2–4] and references therein) and, large seismic activities [5, 6] may affect the sub-ionospheric VLF signals as well as contributing to the variability of the ionosphere. One of the important needs of the ionospheric community is to predict the ionospheric variability (hourly, daily, monthly, yearly, or long-term) as accurately as possible to understand the ionospheric behavior. Variability is more in the lower ionosphere (D/E regions) which is also responsible for attenuation of the high frequency (HF) radio signals.

There are several physics-based theoretical models to calculate radio wave propagation in the earth-ionosphere waveguide. Among them, the popular models are the Long Wave Propagation Capability code [7], Finite Difference Time Domain (FDTD) method [8], wave-hop or ray theory method [9–11]. All these models predict or calculate VLF signal strength between a transmitter and receiver pair based on given ionospheric conditions. Ionospheric conditions are provided mostly using a parameterized ionosphere model such as Wait's model [12] or using the International Reference Ionosphere (IRI) model [2]. Each radio wave propagation model has its advantages and disadvantages in calculation VLF signal strength under various ionospheric conditions. However, the accurate prediction or calculation of the VLF signal strength between a transmitter and receiver pair, namely the 24h diurnal variation in high resolution with respect to time is still a very challenging task because of various factors controlling the variability of the lower ionosphere and variability of the VLF signal especially in the night and dusk/dawn hours.

On the other hand, machine learning models in the framework of artificial intelligence can do wonder in predicting various ionospheric parameters without knowing details of the physical mechanisms. Various studies were done in the past to predict ionospheric peak electron density (NmF2), peak height (hmF2), critical frequency (foF2), total electron content (TEC) using an artificial neural network (ANN) model [13–18]. Santosa & Hobara (2017) applied machine learning to VLF signal such as Nonlinear Auto-regressive with Exogenous Input Neural Network (NARXNN) to predict daily averaged nighttime VLF signal amplitude one day in advance with the Pearson correlation coefficient (r) of 0.93 and Root Mean Square Error 31 (RMSE) of 2.02 dB. They considered stratospheric temperature, total column ozone, cosmic rays, Dst, and Kp index as the inputs of the model. However, predicting the whole

diurnal variation of VLF signals using a machine learning model has never been attempted.

In this paper, for the first time, we have used two supervised machine learning techniques, such as multiple linear regression (hereafter, MLR) and artificial neural network (hereafter, ANN), to model the complex behavior of sub-ionospheric VLF signals, especially the diurnal pattern. The whole process has VLF electric field as target parameter and the parameters affecting the lower ionospheric variations which in turn affect the VLF signal variations, such as F10.7 solar flux, Cosmic ray, solar zenith angle, geomagnetic Dst index, and D-region electron density profiles from the IRI-2016 model, are considered as inputs to the models.

2. DATA AND METHODOLOGY

2.1. INPUTS AND OUTPUT

In this present work, we have considered VLF diurnal variation at 18.2 kHz from the VTX transmitter. The vertical component of VLF electric fields was recorded by Near-Earth Space and Atmospheric Observatory (NESAO) at Kolkata using a 3.65 m E-field whip antenna. VLF signal amplitudes are influenced by variations in the conductivity profiles of the lower ionosphere, namely the D-region ionosphere due to solar and extra-terrestrial inputs (such as Solar Lyman alpha, Soft X-ray, Cosmic ray, etc.). During geomagnetic storms, energetic particle precipitation in the ionosphere also change the ionospheric profiles and disturb the VLF signals [20, 21]. Atmospheric forcing from below the ionosphere also modulates the ionospheric conductivity profiles [22] and therefore VLF signals [23]. But, the major factors that determine the VLF diurnal variation for a particular transmitter-receiver propagation path are solar inputs and corresponding conductivity profiles of the D-region ionosphere. Though the shape of the VLF diurnal variation depends particularly on the propagation characteristics and transmitter-receiver distance [24, 25]. Fig. 1a shows the hourly averaged (red in online version) VLF electric field amplitude (dB) from 25 April 2019 to 06 May 2019 as received in Kolkata. The inset of Fig. 1a shows 24h variation of signal amplitude more clearly with 1 min time resolution in UT (black solid) along with an hourly averaged (red dotted in online version) signal over that. The amplitude minimum between 1-2 UT is generally known as sunrise terminator time minimum (SRTm) which formed due to the destructive interference between the propagating electromagnetic modes when the sunrise terminator sweeps the propagation path from the receiver to the transmitter. The amplitude minimum between 11-12 UT is known as sunset terminator time minimum (SSTm) and after SSTm the signal amplitude increased due to the modal interference between daytime and nighttime modes as the sunset terminator sweeps the propagation path from the receiver

to the terminator. Between SRTm and SSTm, the amplitude follows the solar zenith angle variation. From 14-23 UT, complete night condition over the propagation path ensures the rapid fluctuations of the signal amplitude compared to the daytime.

Here, we have considered five types of inputs, namely the hourly values D-region electron density profiles, F10.7 solar flux, Dst index, solar zenith angle, and Cosmic ray. The hourly values of D-region electron density profiles at altitude range 65 km to 90 km in steps of 5 km are obtained from the IRI-2016 Fortran code (available from http://irimodel.org) over the receiver and mid-point of the transmitter-receiver great circle path (TRGCPm). Thus, the IRI electron density itself served as 12 inputs (6 inputs for receiver and TRGCPm respectively) of the ML models. The fifth panel of Fig. 1b shows the variation of D-region electron density over the receiver at an altitude of 70 km (solid line) and 80 km (dashed line) as an example for the duration 25 April-6 May 2019. Hourly averaged F10.7 solar flux (second panel) and Dst index (third panel) data are obtained from the Space Physics Data Facility of NASA, USA (https://omniweb.gsfc.nasa.gov). Hourly averaged Cosmic ray flux (fourth panel Fig. 1b) is downloaded from the Athens Cosmic ray station (http://cosray.phys.uoa.gr). We also consider the daytime solar zenith angle variation as shown in the first panel of Fig. 1b. Fig. 2, shows the schematic of the simulation setup. In the following two subsections, we describe the two ML models.

2.2. MULTIPLE LINEAR REGRESSION

The regression analysis helps to predict the trends and future values from the existing data. In the context of regression models, the simple linear regression (hereafter LR) is one of the most basic and common predictive analysis models. LR is used mainly to predict the relationship between independent (known as input/s) and dependent variables (known as output) assuming a linear relationship between those input/s and output. If there is a single input variable, then the model is referred to as LR, while there are multiple input variables, the same is termed as a multiple linear regression model (MLR). In both LR and MLR, the output will be a single variable. For MLR, it is accustomed that the inputs are not directly correlated with each other rather, inputs should be independent of each other and random in nature. The distribution of regression residuals is a normal distribution. In Fig. 3a, the schematic diagram for both the LR and MLR are given. Here, x and $(X_1, X_2, ..., X_n)$ are input/s for LR and MLR restively,while,Y is the output for both LR and MLR.

2.3. ARTIFICIAL NEURAL NETWORKS

The term Artificial Neural Networks (ANN) is analogous to the human brain. It includes the computational approach which is inspired by the structure of the human brain. The human brain consists of many neurons connected to each of their

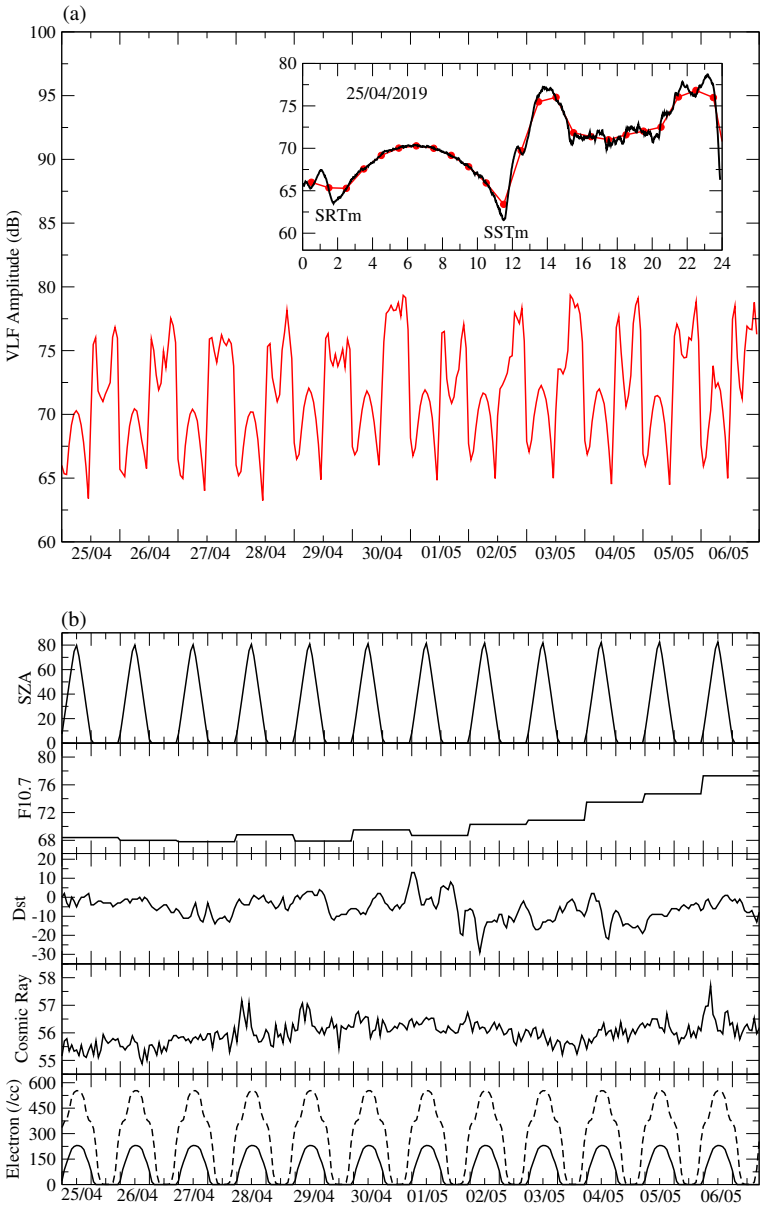

Fig. 1 – (a) Diurnal variation of VLF transmitter signal as output (target) parameter and (b) Various input parameters.

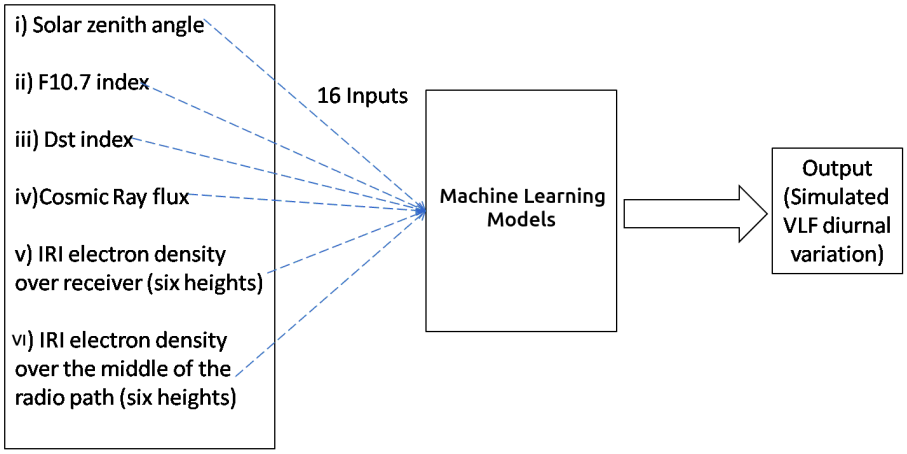

Fig. 2 – Schematic diagram of the simulation set up.

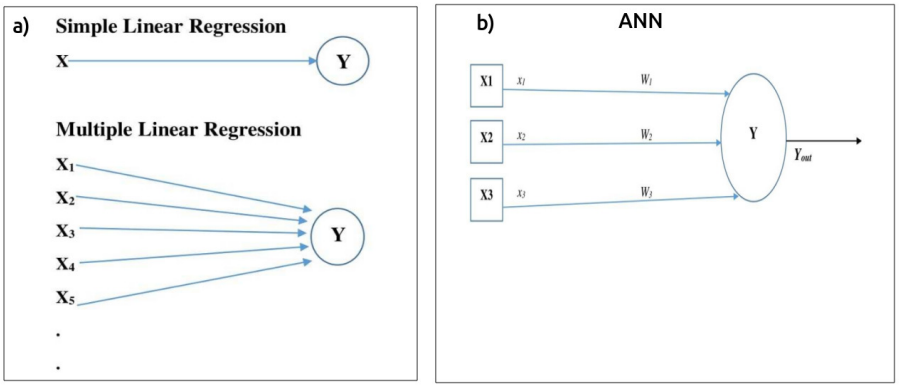

Fig. 3 – Schematic diagram of MLR and ANN.

neighbors. In the human brain, each neuron passes the input signal from one to another as well as passes the information that is to be computed for output. Similarly, the ANN also passes the input signal from one neuron to another and create a network of artificial neurons for computation. The basic structure of the ANN is given in Fig. 3b. A simple ANN structure consists of a n number of inputs and a single output process. Let, (X_1, X_2, X_3) are three inputs process and Y is the output process. Again, each of the input process contains one input signal,say,(x_1, x_2, x_3) along with their corresponding weights $(W1, W_2, W_3....., W_n)$ interconnected with output process. However, there may be more than one output process. Now, for all input process, the net input to the output process is defined as Y_in. The net output Y_{out} is a function of Y_{in}. For a simple ANN, the net output is considered as a binary step function which is given below.

$$Y_{in} = x_1W_1 + x_2W_2 + ... + x_nW_n = \sum_{1}^{n} x_iW_i$$

$$Y_{out} = f(Y_{in}) = \begin{cases} 1 & \text{if } Y_{in} > 0 \\ 0 & \text{if } Y_{in} \leq 0 \end{cases}$$

All the neurons in ANN build the layers or network by interconnecting themselves. These interconnections may or may not be fully connected. According to this layered architecture the ANN can be classified into various divisions, viz, single layer feed-forward ANN, multi-layer feed-forward ANN, competitive network, and recurrent network. All of these networks may have one or more hidden layers with the input and output layers. The output only generates from an output processing unit when a special function satisfies the required criteria for given input variables. This special function that maps the net input value to the output signal values is known as the activation function of that output unit of the ANN.

3. RESULTS AND DISCUSSION

Here, we discuss the simulation results obtained from the two ML models and also compared them with the theoretical models.

3.1. MLR ANALYSIS

MLR is the most common but powerful prediction technique in the context of supervised machine learning. As mentioned in the methodology section, the input and output data are segregated into two sets randomly. In general, among these two sets, the larger set contains more than 50 % of the data which is termed as training data, while the rest set containing less than 50% of data is known as test

data. The data (less than 50%) which was not used during training, are used only for the testing phase. It is relevant to mention here that our training data consist of the data from 25 April to 06 May 2019 to increase the size of training data. On the other hand, to predict VLF, test data are used for May 07-09, 2020. In Fig. 4, the scatter plots of both observed (upper panel) and predicted (lower panel) are shown. To avoid complexity, we used linear regression lines for both the data. Hence, the MLR model reduced the multivariate problem into a simple regression problem with predicted output as a function of observed VLF amplitude. The upper panel of Fig. 4 shows the linear regression between the predicted output and observed values during the training phase with the regression coefficient of $R = 0.9488$. The testing phase produced a regression coefficient of 0.9303. As both of the regression coefficients are close to 1, we can easily conclude that the prediction using MLR is significantly well for the present data.

Now, we will present our predicted VLF for 07-09 May 2020 using the trained model. In Fig. 5, we plotted both the MLR predicted VLFs (red curve) and corresponding observed VLFs (black curve). Unfortunately, we don't have any observed data after 11 UT of 08 May 2019 due to power failure. It is evident from the daytime signal amplitude comparison that the MLR prediction for the first 24 hours i.e., on 07 May is better than the next 24 hours on 08 May. Though the timings of both the minima around sunrise (near $\sim$2 UT) and sunset (near $\sim$12 UT) match well with the observation, amplitude during sunrise minimum tend to overshoot the observation. During night hours ($\sim$14-23 UT), the predicted VLF signal amplitude approximately follows the same pattern as the observation but, there is a mismatch between the observed and predicted amplitude values, which is responsible for the regression coefficient $R = 0.9488$ and $R = 0.9303$ during training and testing phases. Daytime prediction in between $\sim$2-12 UT is very good and matches very well with observation.

3.2. ANN ANALYSIS

We have used a multi-layer perceptron ANN to predict the sub-ionospheric VLF transmitter signal. The 16 variables, as discussed in the previous section, have been used as primary inputs of the model. Levenberg-Marquardt (LM) algorithm [26, 27] has been used to train the neural network. After performing several test runs and analyzing the performance along with regression values, we found that the architecture with one hidden layer that contains seven neurons gives the best results. During the training process, the total data from 25 April to 06 May 2019 (288 data points) are divided into three parts, namely training (70% of 288 data points), validation (15% of 288 data points), and testing (15% of 288 data points). It is relevant to mention here that the distribution (70+15+15) is standard in the context of super-

vised machine learning. However, one may also let this distribution as 80+10+10 etc. The ANN model used the training data set to obtain the nonlinear relationship between input parameters and the target VLF electric field. The validation set, which is not used during training, is used to optimize the network performance, and the testing data set is used to assess the network performance only. The best validation performance is obtained with mean squared error MSE = 1.438, while the same for the training set is MSE=1.432. Fig. 6 shows the linear regression coefficient (R) between the target (observed VLF filed) and ANN output during training, validation, and testing phases. The bottom right of Fig. 6 shows the regression between the predicted and target parameters for all the data. The colored solid lines represent the fit of the corresponding predicted values, and the regression values are shown on the top of each panel. The regression values of the training phase (R=0.9525) and the validation phase (R=0.9515) indicate a good fit between the target and model output. The regression values of the test phase (R=0.9332) and all data (R=0.9495) also indicate a significant linear relationship between the target and model output.

After the training, validation, and testing phase, the trained model is examined for learning efficiency with a new set of input data for 07-08 May 2019. The predicted output (red dashed in on-line) is then compared with the actual observed VLF amplitude data (black in on-line) for the same 48 hours in Fig. 7. Observed data were absent from sunset terminator time minimum around 11 UT for 08 May 2019. We can see that the ANN predicted output is well correlated with the observed values and the linear correlation coefficient between the two is 0.95. Most importantly, the error in prediction or the mismatch between predicted and observed values is relatively large during night hours (between 13-23 UT), while the predicted values are almost accurate for other times. Also, the ANN model captured the two minima around sunrise and sunset (SRTm and SSTm) very well. These results indicate that the learning efficiency and prediction capability of the ANN model are very good for the simulation of diurnal variation of the VLF transmitter signal.

3.3. LWPC SIMULATION

Here, we have calculated the VLF signal amplitude using the most well-known Long Wave Propagation Capability (LWPC) v2.1 code [7]. The LWPC code is a two-dimensional full-wave model for the calculation of amplitude and phase of VLF signals propagating in the Earth-ionosphere waveguide. The lower waveguide boundary is characterized by the permittivity (ϵ) and conductivity (σ) of the Earth surface along the radio propagation path between a transmitter and a receiver pair. The ionospheric conditions can be specified by the altitude profiles of electron and ion density and the collision frequency profiles between electrons, ions, and neutrals. The electron density (N_e) and electron-neutral collision frequency (ν_e) profiles are

sufficient to model the VLF signal variations [28]. Here, we have used the FORTRAN code of the International Reference Ionosphere model IRI-2016 to get the electron density profiles in the altitude range 65-100 km along the radio propagation path used as inputs to the LWPC model. The electron-neutral collision frequency (ν_e) profile as functions of altitude (h) for the D region ionosphere reads as [12], $\nu_e(h) = 1.816 \times 10^{11} exp(-0.15h)$ in sec^{-1} and is default to the LWPC model. The propagation path has been divided into 15 path segments partly based on ground conductivity. The LWPC code has been coupled and automatized with the IRI-2016 model to calculate the radio signal taking inputs for the path segments from the IRI-2016 model along the propagation path. This process was also described in [2, 28]. Then we ran the range-table model of the LWPC code for the VTX-Kolkata propagation path to calculate the diurnal variation of the VTX amplitude at 18.2 kHz with electron density (N_e) and electron-neutral collision frequency (ν_e) along the path. In Fig. 8, we present the IRI-LPWC calculation of the diurnal variation of VTX signal amplitude for the receiver placed at Kolkata by dashed line (red in on-line) corresponding to 07 May and 08 May 2019. The observed variation is indicated by the solid circled line (black in on-line) line. As can be seen from the figure, the IRI-LWPC calculation predicts the SRTm position in the diurnal variation almost at the same time, but the position of the SSTm is delayed by ~ 1 h and also the IRI-LWPC with the default collision frequency predicts slightly lower amplitude at noon. To compare this calculation with the ML models developed earlier, we have plotted the MLR and ANN predictions of the signal amplitude in the same Fig. 8 with the dot-dashed (green in on-line)) and solid (blue in on-line) lines respectively. Thus it can be seen that the ANN and MLR models perform better than the IRI-LWPC model and the ANN model is best among the three. All the model predictions failed to reproduce the variation of the nighttime signal amplitude as the nighttime ionosphere is highly variable with respect to time and space mainly due to the absence of a dominating ionizing sources like the Sun in the daytime.

4. SUMMARY AND CONCLUSION

VLF signal is one of the most important diagnostic tools to monitor the lower part of the ionosphere below 90 km altitude. Continuous monitoring of VLF signals helps to monitor lower ionospheric variability associated with any space weather conditions or other conditions affecting the lower ionosphere. Therefore, their prediction also helps to predict lower ionospheric variability and D-region absorption. In this paper, we have exercised two machine learning models, namely the regression (MLR) and neural network (ANN), for the simulation of diurnal variation of VLF transmitter signal between a transmitter and receiver pair. D-region electron den-

sity variation over the receiver and middle point of the transmitter-receiver path, Dst index, solar zenith angle, Cosmic ray flux, F10.7 solar index are considered as the inputs of the two models. Data from 25 April to 6 May (12 days, 288 data points) are chosen for training and testing purposes. Then using the trained models, we have predicted VLF diurnal variation for 7-8 May 2019. The prediction results are also compared with IRI-LWPC simulation results. It is observed that both the MLR and ANN models simulated the VLF signal variation very well during daytime and dawn-dusk conditions. But the prediction is not good at night. This is because during the nighttime variability of VLF signals is very high compared to daytime as there is no Sun which causes the lower D-region to vanish completely and only weak ionization remained at the upper D-region/lower E-region (above 85 km).

Further, the atmospheric forcing from below dominates the ionospheric variability during nighttime causing VLF signals to fluctuate rapidly compared to daytime. In our model, there are no input parameters that take care of ionospheric variability at night minutely like VLF signals causing a mismatch between hourly observation and prediction during nighttime. The IRI-LWPC simulation also predicted the daytime behavior closely related to the observation except for dusk (during sunset) and night hours. Further, the comparison of all three models indicates that the ANN and MLR models perform better than the IRI-LWPC simulation. Therefore, the studied models can be used to fill the data gaps of sub-ionospheric VLF signals that exist due to power failure or other problems. The present results also indicate that there is a lot of scopes to improve the models for accurate simulation of VLF signals by selecting the input variable wisely at any condition including night. Alternatively, the opposite problem can be exercised to calculate the lower ionospheric electron density variation from the VLF observations which will be reported in our next communication.

Acknowledgments. We thank the scientists and researchers associated with the IRI-2016 model. The IRI-2016 model (source code) was downloaded from http://irimodel.org. Athens's neutron monitor data (http://cosray.phys.uoa.gr) were kindly provided by the Physics Department of the National and Kapodistrian University of Athens. Dst index and F10.7 com solar flux index were obtained from https://omniweb.gsfc.nasa.gov. The VLF data are available from the Near Earth-Space and Atmospheric Observatory, Kolkata (root.nesao@gmail.com).

REFERENCES

1. S. Pal, "Remote Sensing of the Ignorosphere: Need for a Complete Earth-Ionosphere Radio Wave Propagation Model", *Astrophysics and Space Science Proceedings, Springer, Cham.*, **53**, 527–543, (2018).
2. S. Pal, Y. Hobara, S. K. Chakrabarti, P. Schnoor, "Effects of the maj or sudden stratospheric warming event of 2009 on the subionospheric very lowfrequency/low frequency radio signals", *J. Geo. Res. Space Phys.*, **122(7)**,7555–7566, (2017).

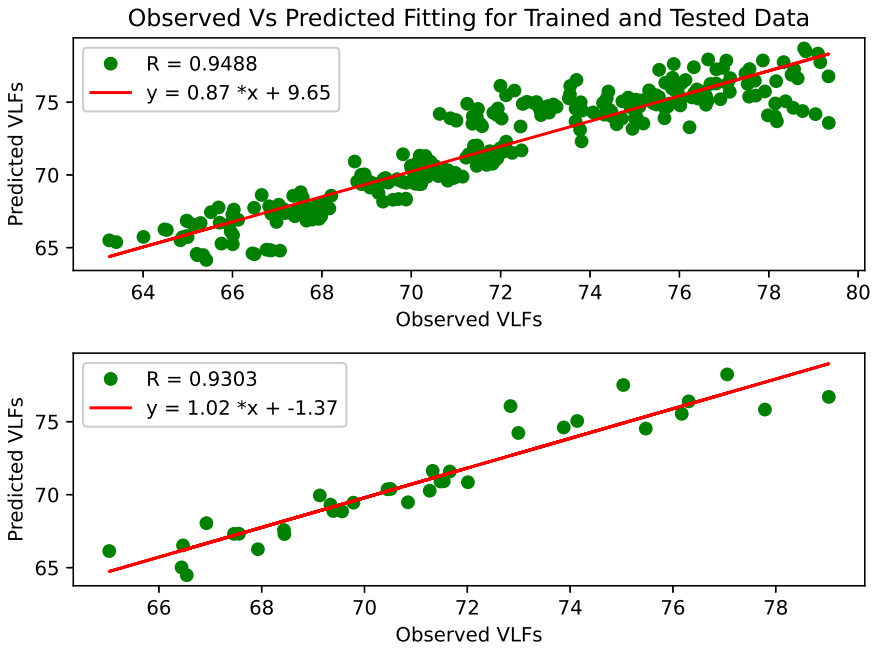

Fig. 4 – Linear regression between the target (observed VLF filed) and MLR output during (a)training, (b)testing phases respectively. Both inputs and target data are considered from 25 April to 06 May, 2014 during training phase and only inputs of 07-08 May, 2019 are considered during testing phase.

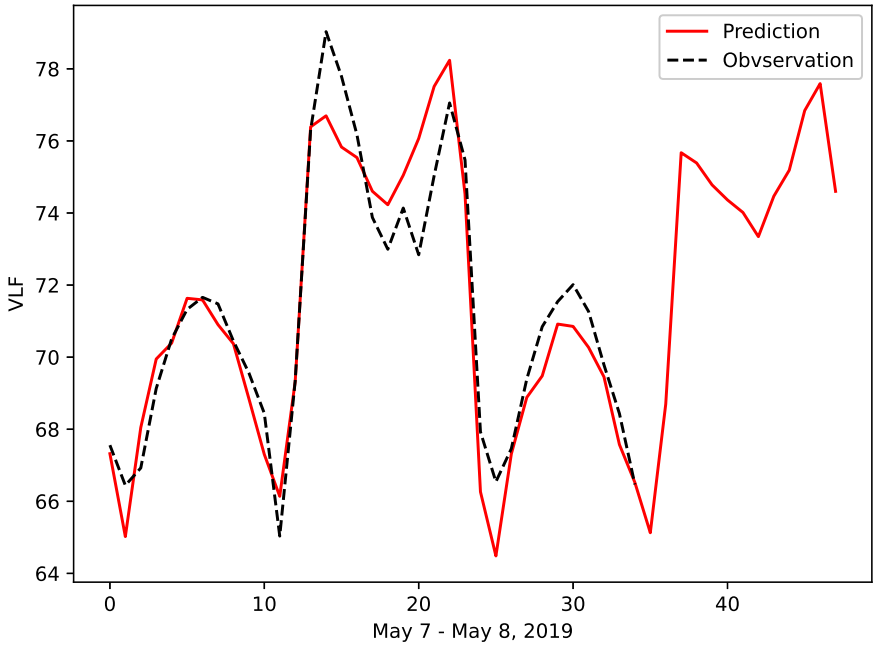

Fig. 5 – MLR model prediction (red) is compared with corresponding observed (black) variation of VLF electric field strength at 18.2 kHz received at Kolkata during 07 May and 08 May, 2019. Both inputs and target (VLF) data from 25 April 2019 to 06 May, 2019 are used for training purpose. There are no observed data after 11 UT of 08 May, 2019 due to power failure.

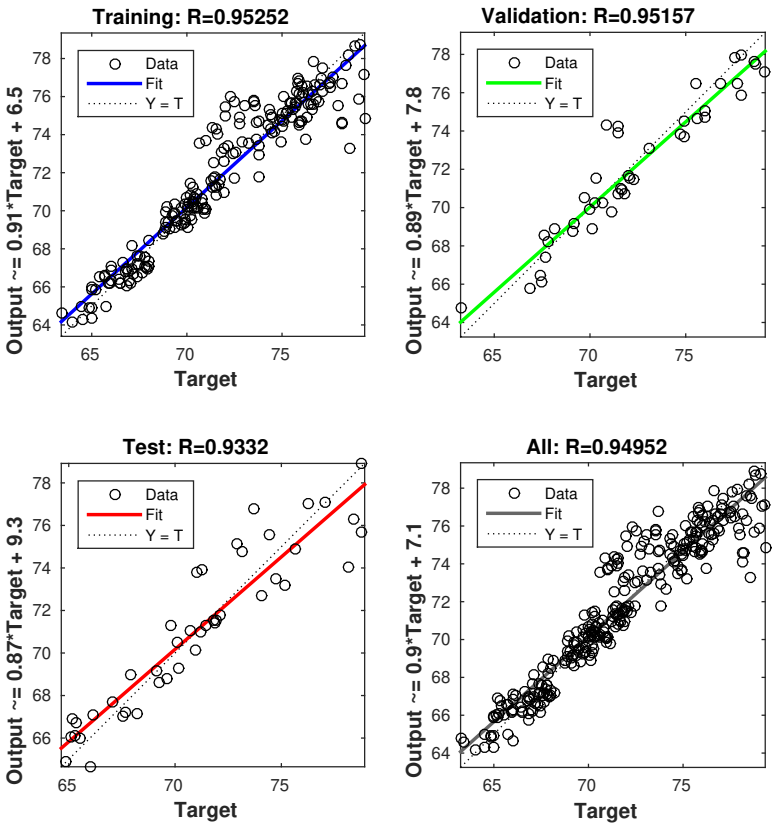

Fig. 6 – Linear regression between the target (observed VLF filed) and ANN output during (a) training, (b) validation, and (c) testing phases respectively. (d) The linear regression between the predicted and target parameters for all the data.

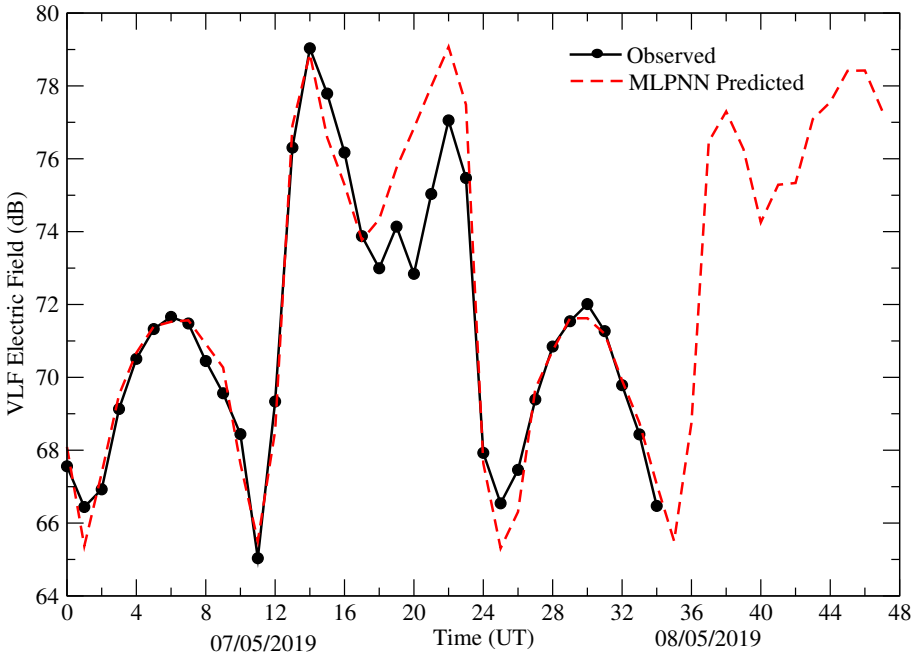

Fig. 7 – ANN model prediction (red) is compared with corresponding observed (black) variation of VLF electric field strength at 18.2 kHz received at Kolkata during 07 May and 08 May, 2019. Here inputs and target (VLF) data from 25 April 2019 to 06 May, 2019 are used for training, validation and testing purpose. VLF field for 07 May and 08 May are predicted completely based on inputs only with the trained model.

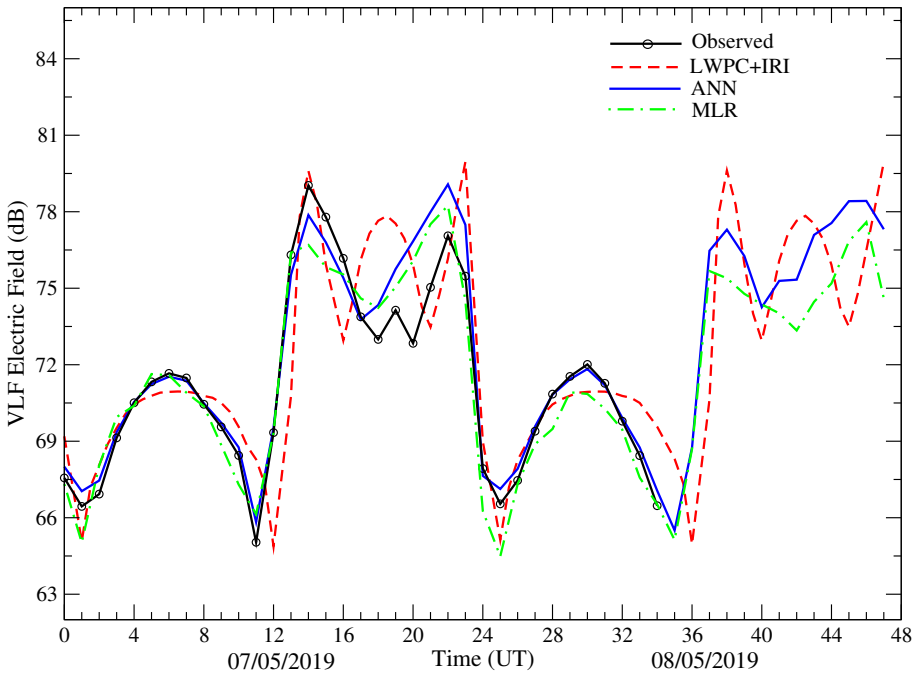

Fig. 8 – Coupled IRI-LWPC model prediction (red) compared with the observation (black) along with the ANN (blue) and MLR (green) model predictions.

3. B. Das, S. Sarkar, P. K. Haldar, S. K. Midya, S. Pal, "D-region ionospheric disturbances associated with the Extremely Severe Cyclone Fani over North Indian Ocean as observed from two tropical VLF stations", *Advances in Space Research*, **67(1)**,75–86, (2020).
4. S. Pal, S. Sarkar, S. K. Midya, S. K. Mondal, Y. Hobara, "Low-Latitude VLF Radio Signal Disturbances Due to the Extremely Severe Cyclone Fani of May 2019 and Associated Mesospheric Response", *J. Geo. Res. Space Phys.*, **125(5)**, https://doi.org/10.1029/2019JA027288, (2020).
5. S. Pulinets, K. Boyarchuk, "Ionospheric Precursors of Earthquakes", *Springer-Verlag Berlin Heidelberg*, (2005).
6. M. Hayakawa, "VLF/LF Radio Sounding of Ionospheric Perturbations Associated with Earthquakes", *Sensors*, **7**, 1141–1158, (2007).
7. J. A. Ferguson, "Computer programs for assessment of long-wavelength radio Communications, version 2.0", *Tech. Document 3030, Space and Naval Warfare Systems Center, San Diego, Calif.*, (1998).
8. D. Inui, Y. Hobara, "Spatio-temporal characteristics of sub-ionospheric perturbations associated with annular solar eclipse over Japan: Network observations and modeling", *XXXIth URSI General Assembly and Scientific Symposium (URSI GASS)*, https://doi.org/10.1109/URSIGASS.2014.6929555, (2014).
9. M. Yoshida, T. Yamauchi, T. Horie, M. Hayakawa, "On the generation mechanism of terminator times in subionospheric VLF/ELF propagation and its possible application to seismogenic effects", *NHESS*, **8**, 129–134, (2008).
10. S. Pal, S. K. Chakrabarti, "Theoretical models for computing VLF wave amplitude and phase and their applications", *AIP Conf. Proc.*, **1286**, 42–60, (2010).
11. S. Pal, T. Basak, S. K. Chakrabarti, "Results of computing amplitude and phase of the VLF wave using wave hop theory", Ed. Kenji Satake, *Advances in Geosciences, Solar Terrestrial*, World Scientific Publishing Company, Singapore, **27**, 1–11, (2011).
12. J. R. Wait, K. P. Spies, "Characteristics of the Earth-ionosphere waveguide for VLF radio waves", *NBS Tech. Note U.S.*, **300**, (1964).
13. O. Altinay, E. Tulunay, Y. Tulunay, "Forecasting of ionospheric critical frequency using neural networks", *Geophysical Research Letters*, **24(12)**, 1467–1470, (1997).
14. T. Maruyama, "Solar proxies pertaining to empirical ionospheric total electron content models", *J. Geo. Res.*, **115(A4)**, https://doi.org/10.1029/2009JA014890, (2010).
15. C. Zhou, R. Wang, W. Lou, J. Liu, B. Ni, Z. Deng, Z. Zhao, "Preliminary investigation of real-time mapping of foF2 in northern China based on oblique ionosonde data", *J. Geo. Res. Space Phys.*, **118**, 2536–2544, (2013).
16. X. Zhao, B. Ning, L. Liu, G. Song, "A prediction model of short-term ionospheric foF2 based on AdaBoost", *Advances in Space Research*, **53(3)**, 387–394, (2014).
17. V. Sai Gowtam, S. Tulasi Ram, "An Artificial Neural Network based Ionospheric Model to predict NmF2 and hmF2 using long-term data set of FORMOSAT-3/COSMIC radio occultation observations: Preliminary results", *J. Geo. Res. Space Phys.*, **122**,11743–11755, (2017).
18. W. Li, D. Zhao, C. He, A. Hu, K. Zhang, "Advanced Machine Learning Optimized by the Genetic Algorithm in Ionospheric Models Using Long-Term Multi-Instrument Observations", *Remote Sens.*, **12(5)**, 866, (2020).
19. H. Santosa, Y. Hobara, "One day prediction of nighttime VLF amplitudes using nonlinear autoregressionand neural network modeling", *Radio Sci.*, **52**, 132–145, (2017).
20. S. A. Cummer, T. F. Bell, U. S. Inan, L. J. Zanetti, "VLF remote sensing of high energy auroral particle precipitation", *J. Geophys. Res.*, **102(A4)**, 7477–7484, (1997).

21. K. Tatsuta, Y. Hobara, S. Pal, M. Balikhin, "Sub-ionospheric VLF signal anomaly due to geomagnetic storms: a statistical study", *Ann. Geophys.*, **33**, 1457–1467, (2015).
22. J. Lastovicka, J., "Forcing of the ionosphere by waves from below", *J. Atmos. Sol. Terr. Phys.*, **68**, 479–497, (2006).
23. S. Pal, S. Chakraborty, S. K. Chakrabarti, "On the use of Very Low Frequency transmitter data for remote sensing of atmospheric gravity and planetary waves", *Advances in Space Research*, **55**, 1190–1198, (2015).
24. S. K. Chakrabarti, S. Sasmal, S. Pal, S. K. Mondal, "Results of VLF campaigns in summer winter and during solar eclipse in indian succontinent and beyond", *AIP Conf. Proc.*, **1286**, 61–76, (2010).
25. S. K. Chakrabarti, S. Pal, S. Sasmal, S. K. Mondal, S. Ray, T. Basak, S. K. Maji, B. Khadka, D. Bhowmick, A. K. Chowdhury, "VLF campaign during the total eclipse of July 22nd, 2009: observational results and interpretations", *J. Atmos. Sol. Terr. Phys.*, **86**, 65–70, (2012).
26. K. A. Levenberg, "Method for the solution of certain non-linear problems in least squares", *Quarterly of Applied Mathematics*, **2(2)**, 164–168, (1944).
27. D. W. Marquardt, "An algorithm for the least-squares estimation of nonlinear parameters", *SIAM Journal of Applied Mathematics*, **11(2)**, 431–441, (1963).
28. S. Pal, "Numerical modelling of VLF radio wave propagation through earth-ionosphere waveguide and its application to sudden ionospheric disturbances", *Ph.D. thesis to University of Calcutta*, arXiv:1503.05789 [astro-ph.EP], (2015).